ACS APPLIED MATERIALS & INTERFACES

Research Article

www.acsami.org

Enhanced Performance of Solution-Processed Amorphous LiYInZnO Thin-Film Transistors

Chang Young Koo,[†] Keunkyu Song,[†] Yangho Jung,[†] Wooseok Yang,[†] Seung-Hyun Kim,[‡] Sunho Jeong,[§] and Jooho Moon*,[†]

[†]Department of Materials Science and Engineering, Yonsei University, 50 Yonsei-ro Seodaemun-gu, Seoul 120-749, Republic of Korea

[‡]School of Engineering, Brown University, Providence, Rhode Island 02912, United States

[§]Device Materials Research Center, Korea Research Institute of Chemical Technology, 19 Sinseongno Yuseong-gu, Daejeon 305-600, Republic of Korea

ABSTRACT: Solution-processed, amorphous lithium-doped YInZnO (L-YIZO) thin-film transistors (TFTs) are investigated. An appropriate amount of Li doping significantly enhances the field-effect mobility in TFT performance (~15 times greater than that of nondoped YIZO) without controlled annealing under water vapor or O_3/O_2 environments. The addition of Li into solution-processed YIZO semiconductors leads to improved film quality, which results from enriched metal oxygen bonding and reduced defect sites, such as oxygen vacancies and hydroxyl groups. Li doping of an amorphous ionic oxide semiconductor (AIOS) could serve as an effective strategy for low-temperature and high-performance solution-processed AIOS TFTs.

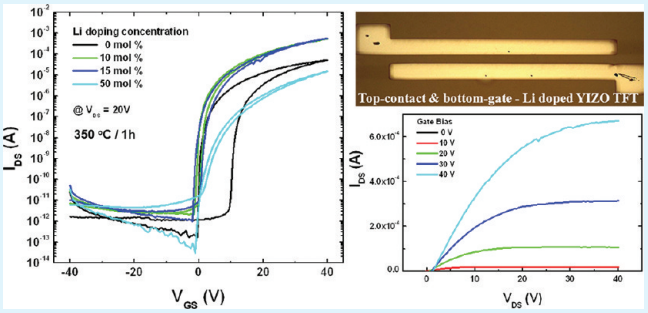

KEYWORDS: *amorphous ionic oxide semiconductor, sol–gel, solution-processed, yttrium indium zinc oxide, semiconductor, thin-film transistor*

1. INTRODUCTION

Ionic oxide semiconductors based on In_2O_3, ZnO, or SnO_2 are attractive for transparent thin-film transistor (TFT) applications due to their wide optical band gap and control of carrier concentrations.[1,2] Recent studies on ionic oxide semiconductors have focused on two viewpoints: an amorphous phase in film form and solution processing in the fabrication method. An amorphous phase is preferred over a crystalline form for device uniformity and low-temperature processability due to its unique carrier transportation mechanism that relies on vacant *s*-orbital overlapping of heavy metal cations, which are relatively insensitive to structural disorder.[3] Various methods have been proposed for the fabrication of amorphous ionic oxide semiconductor (AIOS) TFTs, such as sputtering, pulsed laser deposition, and chemical vapor deposition. However, chemical solution processed depositions are more promising due to their advantages of cost-effectiveness, large area and mass production capabilities.[4,5] Among the chemical solution methods, nontoxic and noncorrosive alcohol-based sol–gel routes with near neutral pH and long-term shelf life stability are promising because of their simple and environmentally benign usages. Furthermore, the sol–gel-derived films have better surface morphology and uniformity.[6,7]

In the case of a sol–gel solution, the metal–oxygen–metal (M–O–M) frameworks form via hydrolysis and condensation reactions. Therefore, it is possible to create oxide thin films at relatively lower processing temperatures compared to those of the metal organic deposition (MOD) methods in which the metal organic (M–R) precursors are thermally decomposed and oxidized at an elevated temperature.[8] Despite the formation of partial M–O–M frameworks in the sol–gel chemistry, the as-deposited film contains organic residues because the sol–gel solution involves a large volume fraction of complicated, chemically bonded organic moieties with cations. The residues originate from the solvents used to dissolve the metal precursors, additives for stabilizing the precursor solutions, and ligands incorporated in the metal precursors. In this regard, the selection of each chemical is an important factor for designing the sol–gel precursors and the process conditions for high-performance, functional oxide thin films.[8,9]

Among the ZnO-based binary and ternary oxide systems reported, indium zinc oxide (IZO) is a candidate material for low-temperature, solution-processed amorphous semiconductors with high electron concentration that can be easily controlled by composition. However, an excess carrier concentration would deteriorate the mobility and TFT performances with unclear switching behavior due to the carrier scattering and defects.[10] To resolve this drawback, we

Received: December 2, 2011
Accepted: February 6, 2012
Published: February 6, 2012

introduced various stabilizers to the amorphous IZO semiconductors as dopants. Typical stabilizers include elements that have a higher ionic valence than that of Zn (+2), such as Ga, La, Sc, Y in Group III and Sn, Si, Hf, Zr in Group IV.[11−13] These elements retain strong bonding characteristics with an oxygen ion, thereby controlling the oxygen deficiencies that may serve as an electron trap or a shallow donor depending on its local structure in ZnO-related AIOS.[2] However, the high ionic valence of a stabilizer presents a difficulty in the precise adjustment of oxygen deficiencies, which makes it difficult to offer a well-controlled carrier concentration, degrading the electrical properties of TFTs. In this study, we introduce a complementary approach through doping with an additional metal cation of low ionic valence. Lithium (Li, ionic valence +1) was selected as an additional dopant, whereas yttrium (Y, ionic valence +3) serves as a main stabilizer in the IZO semiconductor system. We investigate the electrical performance of solution-processed, amorphous Li-doped Y−In−Zn oxide (L-YIZO) TFTs as a function of the doping concentration based on the chemical structure information determined by X-ray photoelectron spectroscopy (XPS) analysis.

2. RESULTS AND DISCUSSION

2.1. Thermal, Chemical, and Electrical Analysis for YIZO Semiconductors. In our previous report, the best device performance of IZO TFTs with clear switching behavior was achieved when the chemical composition of In:Zn was 1:1.[7] In additional preliminary study, a YIZO TFT with Y doping greater than 5 mol % exhibited device performance instability, such as a shift in threshold voltage and reduced field-effect mobility during repeated measurements. As a result, we selected an In:Zn composition ratio of 1:1 with 3 mol % Y doping. All the precursor materials used in the current set of experiments contained the same ligand (i.e., the acetate functional group) to reduce variations in decomposition kinetics and temperatures; otherwise, they varied depending on the ligand type. Figure 1

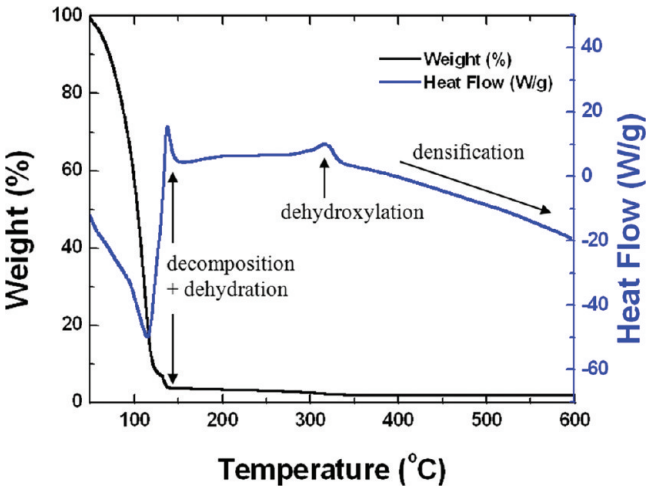

Figure 1. TGA and DSC curves of the YIZO precursor solution with a concentration of ∼0.15 M and composition ratio ∼3 mol % Y-doped IZO (In/Zn molar ratio ∼1:1).

shows the thermal behavior of 3 mol % Y-doped InZnO sol−gel solution with an In:Zn atomic ratio of 1:1. The considerable weight loss accompanying the endothermic reaction at ∼120 °C resulted from the evaporation of the main solvent. An additional small exothermic weight loss reaction that occurred at ∼140 °C is ascribed to thermal decomposition of the complex ligands from the stabilizing agent and acetate functional group. The exothermic reaction at 320 °C is attributed to dehydration and dehydroxylation.[14] Thermal analysis of the YIZO sol−gel solution indicates that the semiconducting characteristics would manifest after annealing at temperatures above 320 °C because annealing below this temperature results in insufficient decomposition of the complex ligands and incomplete dehydration/dehydroxylation, which act as barriers to charge carrier accumulation and transportation in the conduction band.[9,15] As shown in Figure 2a, the TFT annealed at 300 °C was nearly inactive, whereas the TFT annealed at 350 °C had clear switching behavior. The transfer characteristics of the YIZO TFT annealed at 350 °C had a field-effect mobility of ∼0.23 $cm^2\ V^{-1}\ s^{-1}$, a threshold voltage of ∼2.18 V, a subthreshold slope of ∼0.22 V $decade^{-1}$ and an on/off ratio of $\sim 3 \times 10^8$.

To further understand the dependence of TFT performance on the annealing temperature, we investigated the chemical structure evolution of the YIZO semiconductors. Panels b and c in Figure 2 show the oxygen (O) 1s XPS spectra of the YIZO semiconductor annealed at 300 and 350 °C for 1 h. The oxygen peaks are deconvoluted to three Gaussian subpeaks centered near 529.9, 531.4, and 532.7 eV, reflecting different oxygen environments. The band at ∼531.4 eV is attributed to oxygen atoms in the vicinity of an oxygen vacancy, whereas the band in lower energy levels at ∼529.9 eV arises from the oxygen atoms bonded with metal ions (M-O) in a fully coordinated environment. The higher energy level band at ∼532.7 eV is assigned to the hydroxyl group (M−OH), because the presence of more electronegative H results in a shift toward higher binding energies.[16] The YIZO film annealed at 300 °C shows a relatively higher fraction of M−OH and a smaller fraction of M-O than the YIZO film annealed at 350 °C, likely due to an incomplete dehydration/dehydroxylation process of M−OH, as supported by the thermal behavior of the YIZO precursor solution. In amorphous ionic oxide semiconductors, the conduction band minimum should be primarily composed of dispersed vacant metal *s*-orbitals with short interaction distances for efficient carrier transport, which can be achieved in ionic metal-oxides but not in metal-hydroxides.[5] Therefore, the TFT with high metal hydroxide content leads to poor transfer characteristics, even though it has high oxygen vacancy content that may contribute to the carrier concentration. In addition, we annealed YIZO film at temperatures up to 500 °C to further investigate the changes in the chemical structures of the films, as shown in Figure 2d. There were no significant changes in the O 1s spectra subpeak fraction from 350−500 °C, although slight changes in the concentration of M−O and oxygen vacancies were observed with increasing annealing temperature. The dehydration/dehydroxylation was nearly complete at annealing temperatures ranging from 300 to 350 °C. Based on the combined evidence of the TGA-DSC results, XPS analysis and electrical performance of YIZO TFTs as a function of the annealing temperature, the minimum processing temperatures of the acetate precursor-derived sol−gel YIZO semiconductors were greater than ∼320 °C, and annealing at 350 °C was required for the complete dehydration/dehydroxylation process of M−OH.

2.2. Li Doping Effects. We investigated the electrical performances of solution-processed, amorphous Li-doped YIZO TFTs as a function of the Li doping. Panels a and b in

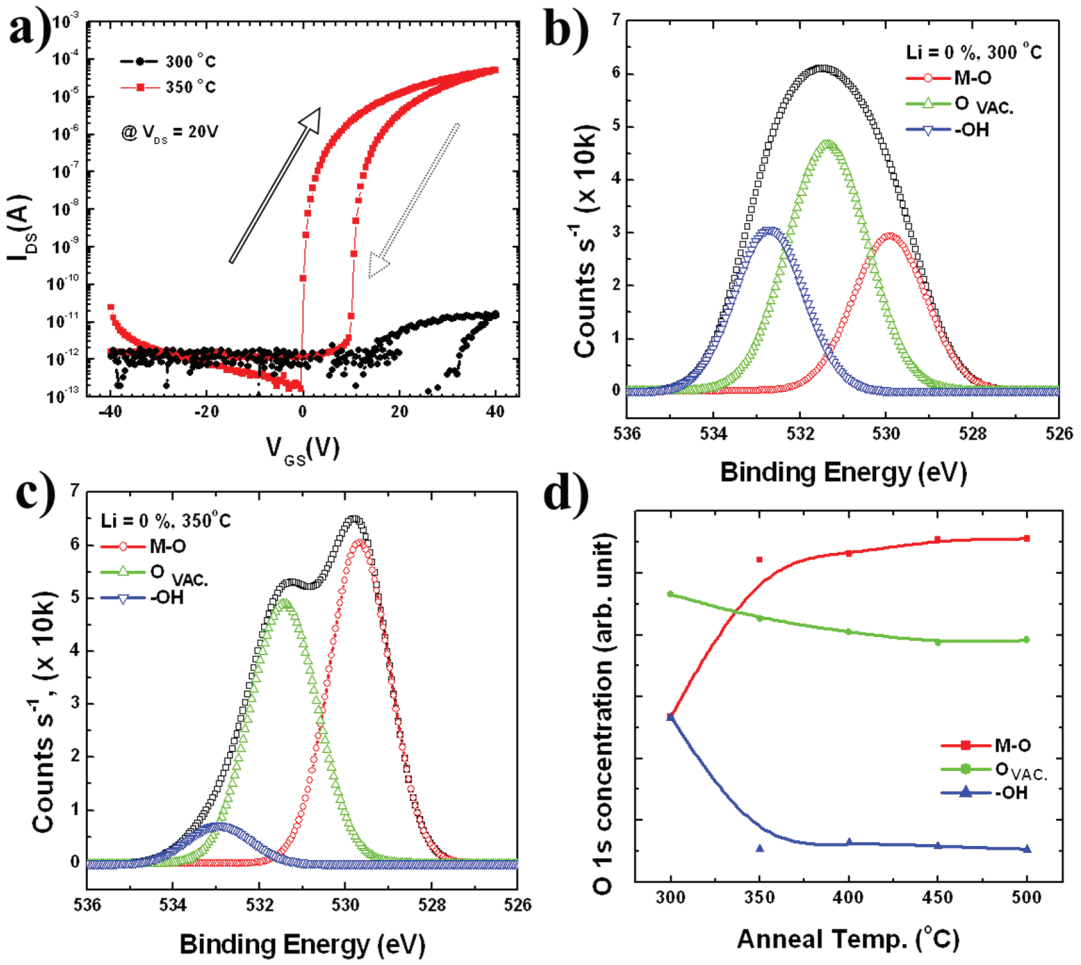

Figure 2. (a) I_{DS}–V_{GS} transfer curves of YIZO TFTs annealed at 300 and 350 °C for 1 h; (b) the concentration profile of each oxygen-related species as a function of the annealing temperatures; (c) the oxygen (O) 1s XPS spectra of the YIZO semiconductor layer annealed at 300 °C for 1 h; (d) O 1s spectra of YIZO annealed at 350 °C for 1 h.

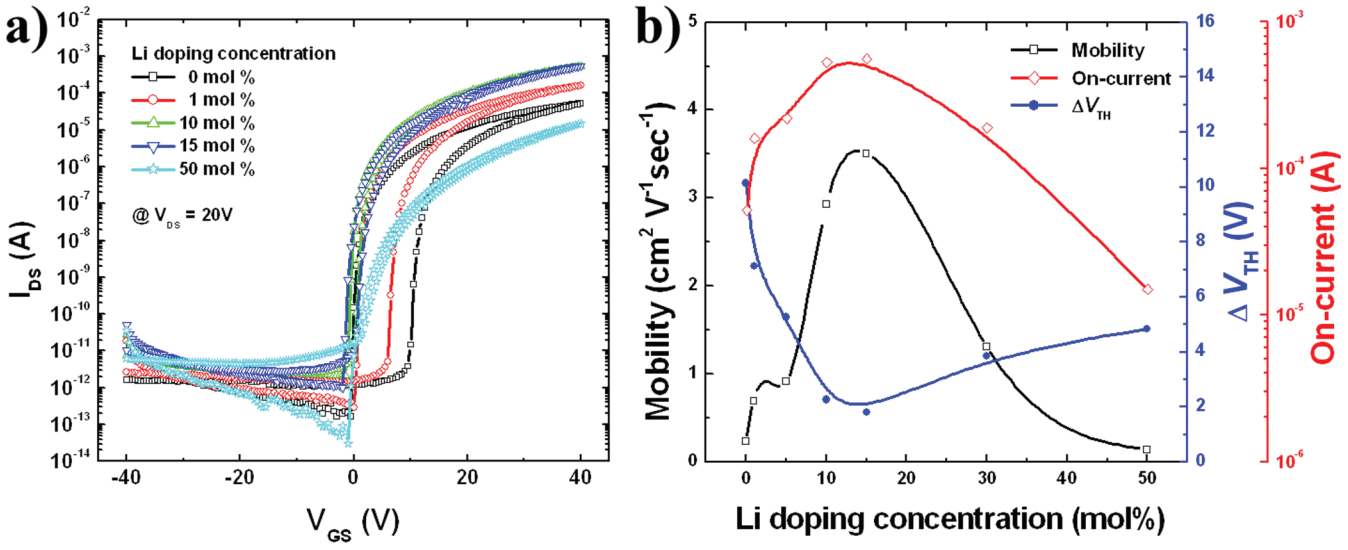

Figure 3. (a) I_{DS}– V_{GS} transfer curves; (b) electrical properties of L-YIZO TFTs as a function of Li doping concentration. All films were annealed at 350 °C for 1 h on a hot-plate in an atmospheric environment and no post-annealing after TFT production.

Figure 3 show transfer characteristics and electrical properties of L-YIZO TFTs (the extracted electrical parameters are shown in Table 1). With increasing Li doping up to 15 mol %, the drain on-current increases from 5.2×10^{-5} to 5.6×10^{-4} A and the threshold voltage variation (ΔV_{TH}) decreases from 10.15 to 1.80 V, whereas the field-effect mobility reaches a maximum of 3.5 $cm^2\ V^{-1}\ s^{-1}$. Lithium has a smaller ionic radius and lower ionic valence (~68 pm, +1) than In (~81 pm, + 3) and Zn

dx.doi.org/10.1021/am201701v | ACS Appl. Mater. Interfaces 2012, 4, 1456–1461

Table 1. Electrical Performance Parameters of L-YIZO TFTs Annealed at 350 °C for 1 h on a Hot-Plate under an Atmospheric Environment

Li doping concentration (mol %)	field-effect mobility ($cm^2\ V^{-1}\ s^{-1}$)	ΔV_{TH} (V)	subthreshold slope (V $decade^{-1}$)	on-current (A)	on/off ratio
0	0.23	10.15	0.22	5.2×10^{-5}	3.1×10^{8}
1	0.69	7.12	0.25	1.6×10^{-4}	5.6×10^{8}
5	0.91	5.27	0.23	2.2×10^{-4}	3.9×10^{8}
10	2.93	2.27	0.30	5.3×10^{-4}	2.4×10^{8}
15	3.51	1.80	0.34	5.6×10^{-4}	5.6×10^{8}
30	1.31	3.84	0.36	1.9×10^{-4}	4.2×10^{8}
50	0.14	4.84	0.42	1.5×10^{-5}	7.5×10^{8}

(~74 pm, + 2), so that the slight doping of Li can be interstitially incorporated into a ZnO-based crystalline matrix depending on the doping level. This incorporation generates charge carriers and enhances the device performance of Li-doped, ZnO-based TFTs.[17] In addition to the role of Li doping on additional charge carrier generation, the chemical structure is varied in sol–gel-derived oxides depending on the dopant concentration, which critically determines the device performance.

XPS analysis of the Li-doped YIZO semiconductors was performed for an in-depth investigation of the relevance of Li doping in the variation of the chemical structure (Figure 4).

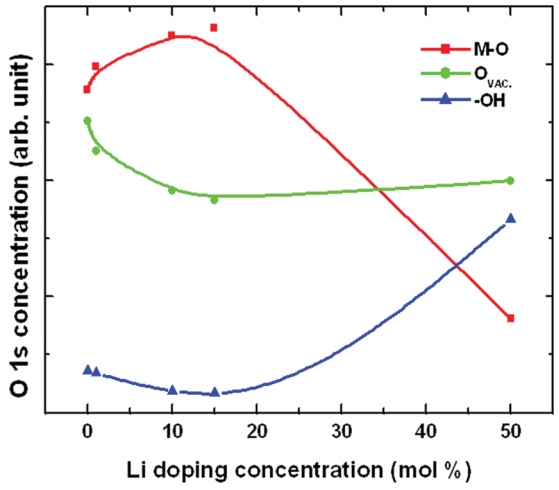

Figure 4. Concentration of each O 1s chemical spectra of the YIZO semiconductor as a function of Li doping concentration. The annealing temperature was 350 °C for 1 h.

Similar to the variation of O 1s XPS spectra in YIZO semiconductors with increasing annealing temperatures, as the Li doping concentration increases to ~15% for the films annealed at 350 °C for 1 h, the relative quantity of M–O increases, and both M–OH species and oxygen vacancy are slightly reduced. The enriched metal–oxygen bonding leads to strengthening of the overlap of vacant metal *s*-orbitals that act as a current path. Hosono et al. reported that, if an oxygen vacancy site in an oxygen-deficient structure is coordinated by a small number of cations or if it is adjacent to a large open space, deep and shallow traps are formed. If an oxygen vacancy site is coordinated by a large number of cations with dense edge-sharing networks, then a shallow donor state is created. However, it has not been proven whether the oxygen vacancy in our LYIZO semiconductor serves as an electron trap or a shallow donor.[18,19] Even though the reduced oxygen vacancy can cause the reduction of the charge carrier concentration which degrades the mobility in TFTs, the mobility does not significantly deteriorate when the charge carrier concentration is slightly reduced. Alternatively, the reduced oxygen vacancy in the AIOS improves the hysteresis behavior in the transfer characteristics, which results from the charge carrier trapping at defect sites in the channel layer. This mechanism has been demonstrated to be enhanced stability of AIOS TFTs by introducing Group III and IV elements as a stabilizer that controls the oxygen vacancy.[11−13,18,20] Therefore, the reduced hysteresis and increased mobility in the transfer curves of LYIZO-TFTs with Li doping up to 15 mol % result from the reduction of the metal hydroxide, which act as trap sites, from the increased overlapping width of vacant metal *s*-orbitals based on enriched metal–oxygen bonding and the reduced defect sites created by an oxygen vacancy in the channel layer.

However, further addition of Li to 30–50 mol % degrades the drain current and saturation mobility, which results from the reduction of metal oxide and enlargement of the metal hydroxide, as shown in Figure 4. In addition, the drastic degradation of device performance may be caused by the segregation of Li in the YIZO semiconductor layer. Figure 5

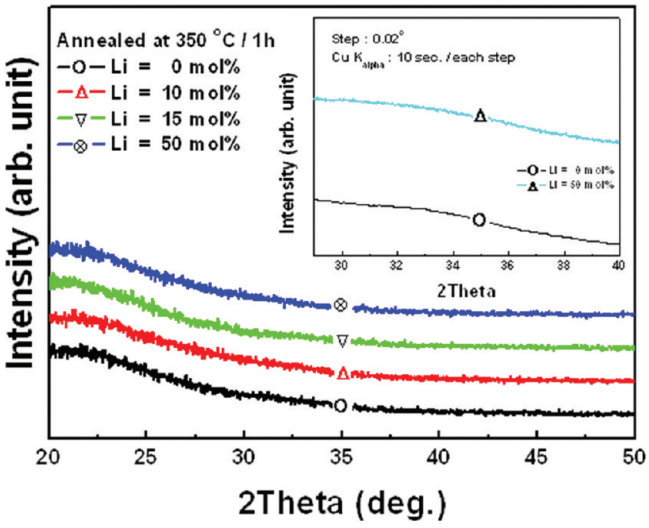

Figure 5. XRD patterns of L-YIZO films as a function of Li doping concentration. Films were annealed at 350 °C for 1 h on a hot-plate under an atmospheric condition (the inset shows XRD patterns of L-YIZO (Li = 0, 50 mol %) films annealed at 500 °C for 1 h).

shows XRD patterns of L-YIZO films annealed at 350 °C as a function of Li doping concentration. All sol–gel-derived films are amorphous and have no secondary phases, regardless of the Li doping concentration. Even when annealed at ~500 °C for 1 h, the films are still amorphous (Figure 5, inset). Banger et al. reported that the films with intermediate In:Zn compositions

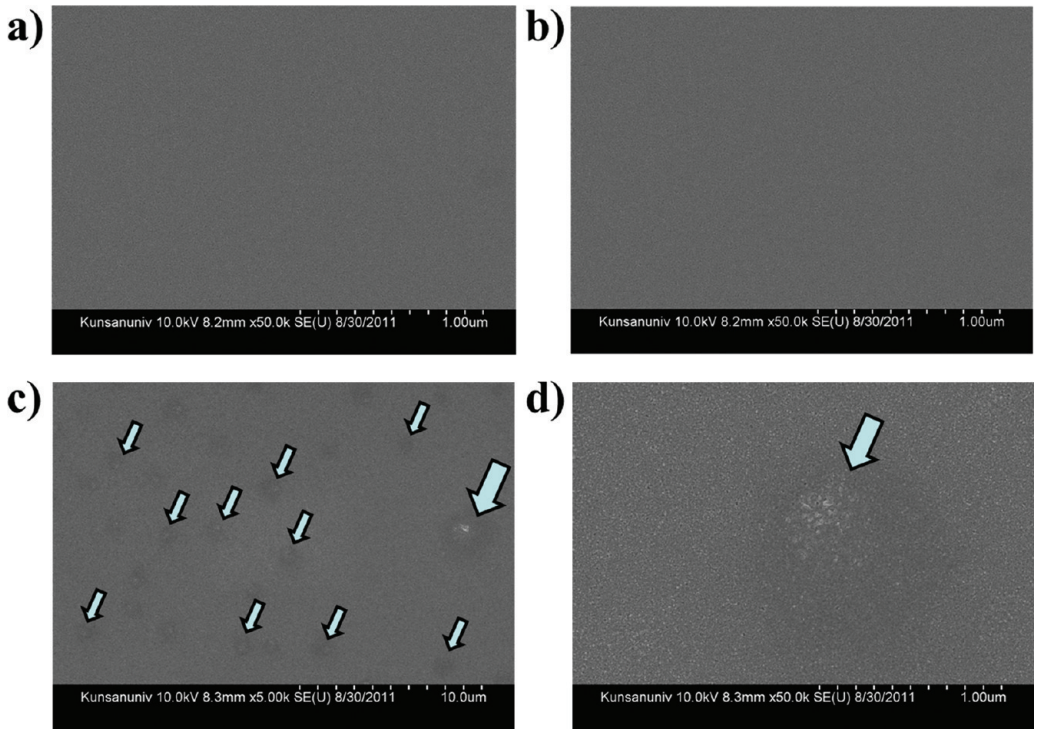

Figure 6. SEM images of L-YIZO films annealed at 350 °C for 1 h on a hot-plate under atmospheric condition as a function of Li doping concentration; (a) Li = 0 mol %, (b) Li = 15 mol %, (c, d) Li = 50 mol %.

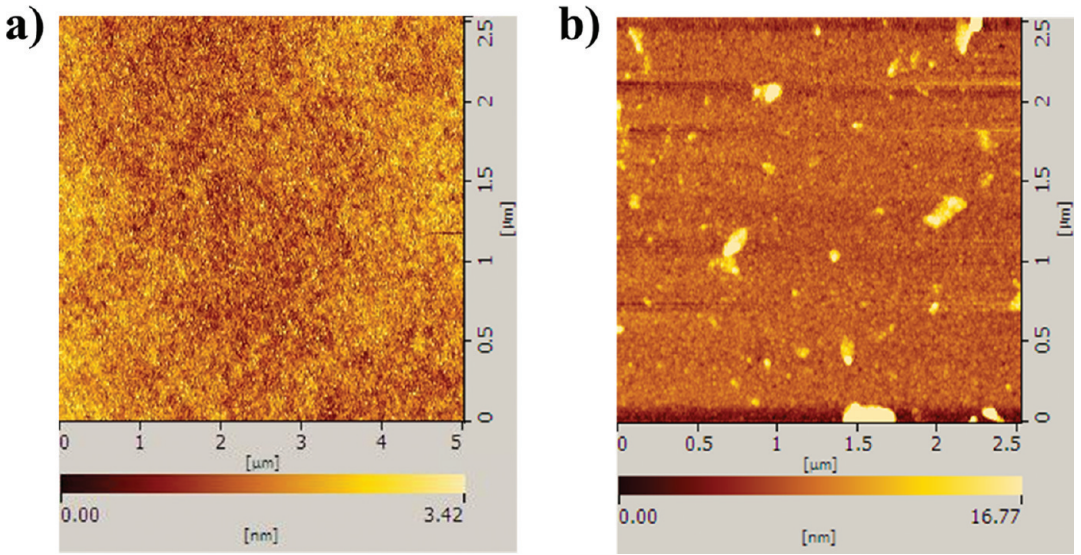

Figure 7. AFM images of L-YIZO films annealed at 350 °C for 1 h on a hot-plate under atmospheric condition as a function of Li doping concentration; (a) Li = 15 mol % and (b) Li = 50 mol %.

ranging from 7:3 to 3:7 were amorphous even when they were annealed at ~550 °C for 2 h under various atmospheres,[8] which corroborates our observation. For a semiconducting channel for large-sized TFTs, an amorphous phase is preferred over a crystalline phase for device performance uniformity. The polycrystalline phase has grain boundaries that lead to the formation of localized interface states, and the number of the grain boundaries within each channel may vary locally, deteriorating the device uniformity.[20]

Even though the absence of secondary phases was confirmed by the XRD analysis, the amorphous secondary phase may be present in Li-doped YIZO layers when a large amount of Li is incorporated into a YIZO film. In this regard, the surface morphologies of L-YIZO films were monitored by a field emission scanning electron microscope. Figures 6 and 7 show the surface morphology of L-YIZO films annealed at 350 °C as a function of Li doping concentration. The L-YIZO films with Li doping up to 15 mol % show clean surface morphologies without secondary phases, but a further increase in Li doping to 50 mol % leads to unknown secondary phases, which may be segregated Li. The segregated Li easily combines with hydroxyl groups (−OH, H_2O) and carbon dioxide (CO_2) during processing in an atmospheric environment because Li is a metal element that has a low ionization energy.[21] The

segregated Li and/or Li-containing compounds act as impurities against charge carrier accumulation and transportation by the impurity scattering mechanism. Therefore, in the case of LYIZO TFTs with excess Li doping, impurity scattering and degraded vacant *s*-orbital overlapping in the channel layer dominantly affect the TFT performances, accompanying the reduced drain current of $\sim 1.5 \times 10^{-5}$ A, low field-effect mobility of ~0.14 $cm^2\ V^{-1}\ s^{-1}$, increased threshold voltage of ~13.64 V, and subthreshold slope of ~0.42.[22,23]

3. CONCLUSIONS

We investigated Li doping effects on the chemical structure of amorphous YIZO semiconductors and electrical performances of TFTs prepared by the sol–gel route and spin-coating method. The results showed that an appropriate amount (~15 mol %) of Li doping in a given composition of a YIZO (Y = 3 mol %, In:Zn mole ratio = 1:1) semiconductor layer and annealing temperature of 350 °C enhanced the TFT performances due to the enriched metal–oxygen bonding and the reduction of both hydroxyl group-related defect sites and oxygen vacancies. The greatest performance was achieved with a 15 mol % Li-doped YIZO-TFT, which exhibited the following device characteristics: an on/off ratio of 5.6×10^8, a field-effect mobility of ~3.51 $cm^2\ V^{-1}\ s^{-1}$, a threshold voltage of ~4.27 V and a subthreshold slope of ~0.34. These results provide a low-temperature, solution-processed AIOS and functional oxide films for successful application in mass-producible electronic devices.

4. EXPERIMENTAL SECTION

4.1. Preparation of Li-Doped YIZO Sol–Gel Solutions. The sol–gel precursor solution for Li-doped YIZO was prepared using metal acetates, including lithium acetate dihydrate [$Li(CH_3COO)\cdot 2H_2O$], yttrium acetate hydrate [$Y(CH_3COO)\cdot H_2O$], indium acetate [$In(CH_3COO)_3$], and zinc acetate dihydrate [$Zn(CH_3COO)\cdot 2H_2O$]. The precursors were dissolved in 2-methoxyethanol at ~90 °C, and a small amount of diethanolamine (DEA) was added to the precursor solution for long-term solution stability. The concentration of the Li-doped YIZO solution was 0.15 mol/L, and the relative molar doping concentration of Li was 0, 1, 5, 10, 15, 30, 50 mol % into 3 mol % Y-doped InZnO (In:Zn = 1:1).

4.2. Preparation of Li-Doped YIZO Semiconductor Layers and Thin-Film Transistors. Li-doped YIZO thin-films (~20 nm) were deposited on a 200 nm thick SiO_2/Si (heavily n-type doped) using a spin-coating method. The films were dried at 200 °C for 10 min to remove residual organics and annealed at 300–500 °C for 1 h on a hot-plate in an atmospheric environment. The top-contact source and drain electrode (50 nm thick Al) was deposited using a thermal evaporation method with a patterned metal shadow mask in which the channel *W*/*L* ratio was 30.

4.3. Characterization. The thermal decomposition behavior of the sol–gel precursors was monitored under an ambient atmosphere using thermal gravimetric and differential scanning calorimetry (TG-DSC, Q600, TA Instruments). The film crystallinity was determined using a multipurpose attachment X-ray diffractometer (Rigaku D/MAX-2500, and PANalytical MPD for thin film), and the surface morphology was monitored by a field emission scanning electron microscope (Hitachi S-4800) and atomic force microscope (Seiko Instrument SPA-400). The electrical performances of Li-doped YIZO TFTs were measured using a semiconductor parameter analyzer (Agilent 4155C) source-measure unit. The chemical structures of Li-doped YIZO semiconductor layers were examined by X-ray photoelectron spectroscopy (VG Microtech ESCA2000) using Al Kα radiation (~1486.6 eV), and the carbon 1s peak at ~284.6 eV was used as a reference for calibration.

AUTHOR INFORMATION

Corresponding Author

*E-mail: jmoon@yonsei.ac.kr. Tel.: +82-2-2123-2855. Fax: +82-2-312-5375.

Notes

The authors declare no competing financial interest.

ACKNOWLEDGMENTS

This work was supported by the Mid-Career Researcher Program through an NRF grant funded by the MEST (2009-0086302). It was also partially supported by the Second Stage of the Brain Korea 21 Project.

REFERENCES

(1) Nomura, K.; Ohta, H.; Tagaki, A.; Kamiya, T.; Hirano, M.; Hosono, H. *Nature* **2004**, *432*, 488–492.
(2) Hosono, H. *J. Non-Cryst. Solids* **2006**, *352*, 851–858.
(3) Iwasaki, T.; Itagaki, N.; Den., T.; Kumomi, H.; Nomura, K.; Kamiya, T.; Hosono, H. *Appl. Phys. Lett.* **2007**, *90*, 242114.
(4) Jeong, S.; Ha, Y.-G.; Moon, J.; Facchetti, A.; Marks, T. J. *Adv. Mater.* **2010**, *22*, 1346–1350.
(5) Jun, T.; Song, K.; Jeong, Y.; Woo, K.; Kim, D.; Bae, C.; Moon, J. *J. Mater. Chem.* **2011**, *21*, 1102–1108.
(6) Koo, C. Y.; Kim, D.; Jeong, S.; Moon, J.; Park, C.; Jeon, M.; Jung, J.; Woo, H. J.; Kim, S.-H. *J. Korean Phys. Soc.* **2008**, *53*, 218–222.
(7) Koo, C. Y.; Song, K.; Jun, T.; Kim, D.; Jeong, Y.; Kim, S.-H.; Ha, J.; Moon, J. *J. Electrochem. Soc.* **2010**, *157*, J111–J115.
(8) Banger, K. K.; Yamashita, Y.; Mori, K.; Peterson, R. L.; Leedham, T.; Rickard, J.; Sirringhaus, H. *Nat. Mater.* **2010**, *10*, 45–50.
(9) Jeong, S.; Lee, J.-Y.; Lee, S. S.; Choi, Y.; Ryu, B.-H. *J. Phys. Chem. C* **2011**, *115*, 11773–11780.
(10) Pasquarelli, R. M.; Ginley, D. S.; O'Hayre, R. *Chem. Soc. Rev.* **2011**, *40*, 5406–5441.
(11) Jeong, S.; Ha, Y.-G.; Moon, J.; Facchetti, A.; Marks, T. J. *Adv. Mater.* **2010**, *22*, 1346–1350.
(12) Shin, H. S.; Kim, G. H.; Jeong, W. H.; Ahn, B. D.; Kim, H. J. *Jpn. J. Appl. Phys.* **2010**, *49*, 03CB01.
(13) Chong, E.; Chun, Y. S.; Lee, S. Y. *Appl. Phys. Lett.* **2010**, *97*, 102102.
(14) Kim, D.; Koo, C. Y.; Song, K.; Jeong, Y.; Moon, J. *Appl. Phys. Lett.* **2009**, *95*, 103501.
(15) Kim, M.-G.; Kanatzidis, M. G.; Facchetti, A.; Marks, T. J. *Nat. Mater.* **2011**, *10*, 382–388.
(16) Fan, J. C. C.; Goodenough, J. B. *J. Appl. Phys.* **1977**, *48*, 3524–3531.
(17) Adamopoulos, G.; Bashir, A.; Thomas, S.; Gillin, W. P.; Georgakopoulos, S.; Shkunov, M.; Baklar, M. A.; Stingelin, N.; Maher, R. C.; Cohen, L. F.; Bradley, D. D. C.; Anthopoulos, T. D. *Adv. Mater.* **2010**, *22*, 4764–4769.
(18) Kamiya, T.; Nomura., K.; Hirano, M.; Hosono, H. *Phys. Status Solidi* **2008**, *5*, 3098–3100.
(19) Kamiya, T.; Nomura., K.; Hosono, H. *Phys. Status Solidi A* **2009**, *206*, 860–867.
(20) Kamiya, T.; Nomura., K.; Hosono, H. *Sci. Technol. Adv. Mater.* **2010**, *11*, 044305.
(21) Tanaka, S.; Taniguchi, M; Tanigawa, H. *J. Nucl. Mater.* **2000**, *283–287*, 1405–1408.
(22) Fujihara, S.; Sasaki, C.; Kimura, T. *J. Eur. Ceram. Soc.* **2001**, *21*, 2109–2112.
(23) Nayak, P. K.; Jang, J.; Lee, C.; Hong, Y. *Appl. Phys. Lett.* **2009**, *95*, 193503.